REVIEW ARTICLE

Cerebral Oxygenation Studies Through Near Infrared Spectroscopy: A Review

Shubhajit Roy Chowdhury[1,*], Gaurav Sharma[2], Yashika Arora[3]

[1,2,3]Biomedical Systems Laboratory, School of Computing and Electrical Engineering, Indian Institute of Technology Mandi, India

*Corresponding author: Email: src@iitmandi.ac.in

DOI: 10.5185/amlett.2020.031482

Near-infrared spectroscopy (NIRS) is increasingly becoming popular for monitoring cerebral oxygenation level by measuring the time variations in the concentrations of oxygenated hemoglobin (HbO_2) and deoxygenated hemoglobin (Hb). Studies on cross section of the cerebro-vascular artery suggest that impaired haemodynamics of cerebrovascular artery is followed by transient ischemic attack (TIA) and ischemic stroke. Here, cerebrovascular reactivity (CVR) signifies the dilation capacity of blood vessels, and is a remarkable bio-marker for brain vascular reserve. The CVR may be effectively studied by monitoring cerebral oxygenation level, which if coupled with anodal transcranial direct current stimulation can serve as an important biomarker to classify between stroke and non-stroke patients, thereby providing for an imminent screening and monitoring tool. The neural activity of cerebral cortex may be controlled with transcranial direct current stimulation (tDCS) where the NIRScan be used to capture CVR during anodal tDCS. The responses measured during NIRS are measured through temporal changes in HbO2 and Hb concentration — which provide more information than those available from basic fMRI. This article first reviews the general principles and progress in the development of NIRS, throwing a light on the applications of NIRS in stroke diagnosis.

Introduction

Infrared (IR) spectroscopy is an important analytical technique used in science. IR spectroscopy is based on the vibrations of the atoms of a molecule. Usually, the IR radiation is passed through a sample. The fraction of the incident radiation which is absorbed at a particular energy is estimated. The specific frequencies, at which a sample molecule or its parts vibrate, show energy peaks in the absorption spectrum. When the spectroscopy is carried out in the wavelength window of 800 – 2500 nm wavelength, it is called near-infrared spectroscopy (NIRS). Literature survey reveals that a large number of molecules have absorption peaks because of electronic transitions in the NIR region [**1-10**].

In this review, the "versatility" of NIR spectroscopy in cerebral oxygenation studies is brought out, portraying the recent progress. NIR spectroscopy is very versatile in different ways. Firstly, NIR spectroscopy combines electronic spectroscopy with vibrational spectroscopy. In fact, IR, Raman, and NIR spectroscopy form the "three sisters of vibrational spectroscopy". However, NIR spectroscopy dealing only with overtones and combination mode, is quite unique as compared to IR and Raman spectroscopy. A survey of literature reveals a plethora of applications of Electronic NIR spectroscopy [**11-15**]. Jobsis in 1977 reported the notion of detecting cerebral oxygenation through NIR spectroscopy [**16**]. NIRS based optical recording technology is used to measure the temporal changes in concentrations of oxyhemoglobin (HbO_2) and deoxyhemoglobin (Hb) from the changes in the number of absorbed photons as well as those scattered back to the surface of the scalp. Neuroimaging studies through NIRS is also gaining popularity since the 1990s [**17**], where NIRS is used to assess cortical activity at the time of cognitive and motor tasks in healthy persons as also in persons with damaged central nervous system [**18, 19**]. Because NIRS has good temporal and spatial resolution but no radiation, it is popularly used for the physiological study of muscle [**20**], breast tumors [**21,22**] and also in cerebral blood flow studies in both animal and human beings [**23,24**]. NIRS has also been applied in a wide range of fields, such as cognition science [**18**], neonatology [25], rehabilitation, brain computer interface (BCI) [**26**] and so on.

The paper is organized as follows. In section 2 principles of near infrared spectroscopy has been discussed. Section 3 focuses on the importance of cerebral oxygenation studies. Section 4 focuses on the principles of estimation of cerebral oxygenation using NIRS. Section 5 discusses the effects of extra cerebral tissue on cerebral oxygenation. In section 6, a phenomological model has been described, that has been developed to capture using NIRS, the hemodynamic response to anodal transcranial direct current stimulation. Section 7 describes the design of NIRS based cerebral oximeter.

Principle of near infrared spectroscopy

Infrared (IR) spectroscopy is a useful technique for determining the chemical composition both qualitatively as well as quantitatively. Molecular vibrational transitions measured in the near-infrared (NIR) region (750 to 2,500 nm) can be characterized as multi quanta, single photon and electric dipole transitions. NIR spectroscopy mainly deals with two types of transitions one is electronic transitions and other one is molecular vibrational transitions. In the previous study, there is no clear way find the difference between electronic transitions occurring in the visible and NIR region, although it is known that a larger part of the electronic transitions detected in the NIR region are because of d-d transitions, π-π* transitions, and charge-transfer (CT) transitions of large, or long, conjugated systems. NIR region and IR region can be easily discriminated from each other. This is because NIR deals with only bands due to overtones and combination modes, whereas the IR is mainly concerned with fundamentals. In general, electronic transitions seen in the NIR region have weak bands. Weak bands also arise from overtones and combination modes and are called forbidden transitions [**1-10**]. In fact the notion of forbidden transitions associated with NIR region, leads to uniqueness of this region and makes it reasonably different from the other regions. Only the NIR region serves as a highly transmitting window to radiation. In other neighboring regions, viz. the visible region, the IR region, the far IR region and the ultraviolet region, a number of allowed transitions can occur. In other words, the NIR region is characterized by very weak absorption. The NIR region is typically divided into region I (wavelength ranging from 800 nm to1200 nm), region II (wavelength ranging from 1200nm to 1800 nm) and region III (wavelength ranging from 1800nmto 2500 nm). There is no rigid boundary between the three regions and, in fact one region gradually gives way to the other. Region I is having some very unique features. It is variously called as: “near NIR (NNIR) region”, or “the Herschel region” and “the short-wave NIR (SWNIR) region”. In this region, all the bands are weak. Hence, region I show a very high degree of transparency. Region I is also called “the window of body” [**1-10**]. A number of biomedical and agricultural applications are carried out in this region I. Region I is detected with the help of the charged coupled devices (CCD). Therefore, we see that the different instruments are employed in region I as compared to those used in regions II and III.

Importance of cerebral oxygenation studies

Cerebrovascular accident or stroke occurs due to a ruptured cerebral blood vessel and the resultant brain bursts (known as hemorrhagic stroke) or a clot or embolus that is formed inside the artery which obstructs the flow of blood thereby consequent deprivation of oxygen and nutrients supply to the brain leads to death of brain tissues (known as ischemic stroke). Every year, around 15 million people worldwide suffer a stroke. Studies in India have revealed that the incidence rates have increased from 27-34/100,000 in the age group of 35-44 to 822-1116/100,000 in the age group of 75+ [**27-29**]. Amongst the different kind of strokes, ischemic stroke, by far, is the leading cause of long term disability worldwide causes death with a very high probability [**30**]. Ischemic stroke also causes dementia with the number of dementia cases just following Alzheimer’s disease (AD). In last five decades, the estimated care cost of a patient suffering from brain stroke is reached around trillions of dollar. 10% of death cases and about 5% of health-care costs are contributed by stroke only [**31**]. In United States 2010, the whole care cost of patients suffering from brain stroke and heart attack was estimated to be 315.4 billion dollars [**32**]. The whole care cost divided into two categories direct and indirect care cost. In direct care cost including cost of diagnostics test, physicians and other professionals, hospital services, suggested medicines, home-based health care, and other medical durables. Less efficiency due to indirect care cost that results early death. In India, stroke is much more abundant in younger individuals (18-32% of all stroke cases) as compared to high-income countries which reflect a greater burden on the quality of life [**27**, **33**]. Stroke drastically minimizes the productivity of the youth age group which adds further to the loss [**33**]. With increasing abundance in the number of younger stroke patients and an aging population, the human burden as well as the economic burden of stroke and also small vessel disease will be on a steady rise in future [**34**]. By 2025, the elderly population in India is estimated to increase to 12% of the total population [**35**]. Therefore, innovative low cost point of care technologies for prognosticating patients and diagnosing stroke and small vessel disease are urgently required in developing countries like India to avoid translation and transportation of critical patients and provide for at home mediation.

Cross-sectional studies on cerebrovascular artery reveal that impairment of cerebral hemodynamics precedes transient ischemic attack (TIA) and ischemic stroke. Here, CVR signifies the dilation capacity of blood vessels, and is a good biological marker for the brain vascular reserve [**36**]. CVR provides a good supplement to the state of the art practice of measuring the baseline of blood flow. Here, severe reduction of CVR predicts the risk of ipsilateral stroke and TIA [**36**]. Also, neural activity is closely related to cerebral blood flow (CBF). The CBF supplies glucose via NVC. However, neurological symptoms due to impairment in CBF are typically not visible until the CBF drops to 40% of the normal. Also, sustained cerebral ischemia over prolonged periods increases the probability of neurological symptoms not being reversed as CBF further falls to 20% of normal [**37,38**]. The objective of most clinical interventions in ischemic and acute ischemic stroke care is to increase the blood perfusion in the lesioned region and the surrounding ischemic penumbra by maximizing local and/or global CBF. Intervention strategies for increasing CBF assume that the normal auto-regulation of CBF is

disturbed and blood perfusions of the infarcted and penumbral regions are a function of perfusion pressure [**39,40**]. Here, the direct and indirect measurement of CBF, concentrations of Hb and HbO_2 at the point-of-care would provide new horizons for monitoring cerebro-vascular auto-regulation in TIA, enabling hemodynamic interventions to be potentially administered and optimized neurological symptoms become visible. Furthermore, because of the tremendously high abundance of stroke and small vessel disease patients, and the enormity of cost in its management, strategies with reasonably good benefits would potentially ameliorate impaired CBF that would otherwise cause neural impairments leading to Mild Cognitive Impairment (MCI) [**41**]. Also, impaired cerebral hemodynamics may cause vascular dementia (VD), where the pathophysiological connections between VD and AD have been popularly discussed [**41,42**]. In fact, impaired cerebral micro-vessels functionality (elucidated with CVR) is closely associated with unfavorable evolution of cognitive function in patients with AD [**42**].

Functional near infrared spectroscopy (fNIRS) is based on the notion of optically measuring the variations in HbO_2 and Hb concentration [**43**] in the tissues. Cerebral oximetry refers to cerebral oxygenation monitoring using NIRS device [**44**]. Functional magnetic resonance imaging (fMRI) is closely related to fNIRS with respect to underlying measure and, i.e. cerebral oxygenation level. The fNIRS responses are interpreted in terms of changes in HbO_2 and Hb concentration which constitutes a somewhat richer set of variables than those available from basic fMRI. Total hemoglobin (Hbt) concentration is summation of HbO_2 and Hb concentrations. Hbt concentration is helpful to calculate the variations in the regional cerebral blood flow (rCBF) [**45**].

Principle of cerebral oxygenation estimation using NIRS

The principle of estimation of cerebral oxygenation using NIRS is based on absorbance of a specific blood component at specific body part is showing at particular wavelength in NIR region as achieved by Beer-Lambert's law [**46**] is given as,

$$A(\lambda) = \varepsilon_\lambda cl \tag{1}$$

where is $A(\lambda)$ is the absorbance caused by solute, ε_λ is the absorption coefficients of the solute at a particular wavelength λ, c is the concentration of solute in solution and l is the path length. However, in case of blood there are multiple components. For n different components, the total absorbance is given by:

$$A_{tot} = \sum_{i=1}^{n} \varepsilon_{i\lambda} c_i l \tag{2}$$

Thus, the concentration of the solute can easily be calculated by calibrating the values of path-length l, absorbance $A(\lambda)$ and molar absorptivity ε_λ at a particular wavelength λ. Also, the absorbance $A(\lambda)$ is related with intensities of incident and transmitted radiation as follows:

$$A(\lambda) = \log\left(\frac{I_0}{I}\right) \tag{3}$$

where, I is the transmitted intensity and I_0 is the incident light intensity.

The attenuation of light measured across the scalp depends on source and photo-detector configuration, scalp shape and the scattering and absorption properties of the tissues by a complex relationship. Assuming the tissue being illuminated to be optically homogeneous, source emit light at constant frequency and amplitude, the modified Beer Lambert's law [**46**] needs to be applied:

$$A(\lambda) = \log\left(\frac{I_0}{I}\right) = \varepsilon_\lambda cld_p + G \tag{4}$$

where d_p refers to the differential path length factor and G refers to the scattering loss factor, which are generally unknown. Since G is generally unknown, hence absolute concentrations of chromophores are not derivable, rather their changes can be estimated as:

$$\Delta A_{21}(\lambda) = \log\left(\frac{I_0}{I_2}\right) - \log\left(\frac{I_0}{I_1}\right) = \log\left(\frac{I_1}{I_2}\right) = \varepsilon_\lambda \Delta cld_p \tag{5}$$

where $\Delta A_{21}(\lambda)$ refers to the change in absorption at two different time instants t_1 and t_2.

In case of estimation of blood oxygenation, as in the case of cerebral oximetry, since the absorption bands of Hb and HbO_2 are different, hence equation (5) needs to be solved in two different wavelengths as:

$$\Delta A_{21}(\lambda_a) = ld_p\left(\varepsilon_{Hb_{\lambda_a}} \Delta[Hb] + \varepsilon_{HbO_{2\lambda_a}} \Delta[HbO_2]\right) \tag{6}$$

and

$$\Delta A_{21}(\lambda_b) = ld_p\left(\varepsilon_{Hb_{\lambda_b}} \Delta[Hb] + \varepsilon_{HbO_{2\lambda b}} \Delta[HbO_2]\right) \tag{7}$$

where $\Delta A_{21}(\lambda_a)$ and $\Delta A_{21}(\lambda_b)$ refers to the change in absorption at two different time instants t_1 and t_2 measured at wavelengths λ_a and λ_b respectively. Equations (6) and (7) represent two simultaneous equations with two unknowns and hence can be used to estimate the relative change in cerebral oxygenation over time. **Fig. 1** shows the absorption spectra of Hb and HbO_2.

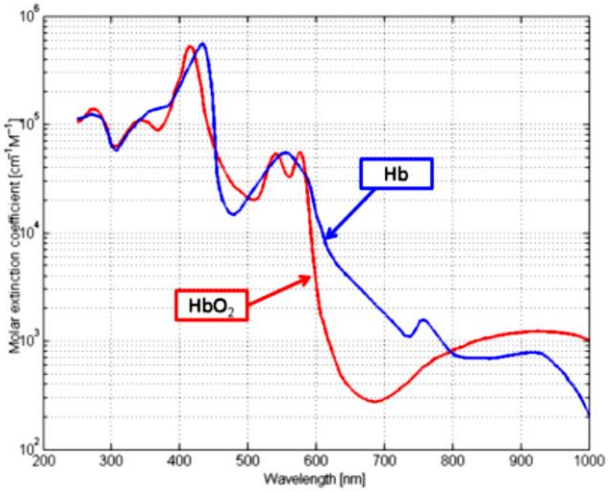

Fig. 1. Absorption spectra of Hb and HbO_2.

However, as evident from **Fig. 2**, at near infrared part of the spectrum, the absorption of radiation by water becomes significant particularly beyond 900nm.

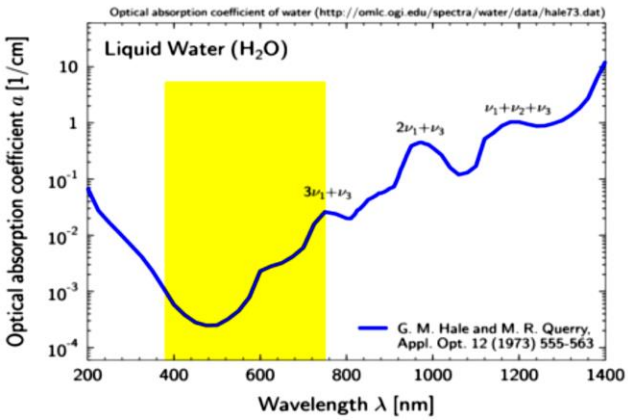

Fig. 2. Absorption spectrum of water.

Hence, equation (6) and (7) needs to be modified incorporating change in concentration of water as:

$$\Delta A_{21}(\lambda_a) = l d_p \left(\varepsilon_{Hb_{\lambda_a}} \Delta[Hb] + \varepsilon_{HbO_{2\lambda_a}} \Delta[HbO_2] + \varepsilon_{H_2O_{\lambda_a}} \Delta[H_2O]\right) \quad (8)$$

$$\Delta A_{21}(\lambda_b) = l d_p \left(\varepsilon_{Hb_{\lambda_b}} \Delta[Hb] + \varepsilon_{HbO_{2\lambda_b}} \Delta[HbO_2] + \varepsilon_{H_2O_{\lambda_b}} \Delta[H_2O]\right) \quad (9)$$

$$\Delta A_{21}(\lambda_c) = l d_p \left(\varepsilon_{Hb_{\lambda_c}} \Delta[Hb] + \varepsilon_{HbO_{2\lambda c}} \Delta[HbO_2] + \varepsilon_{H_2O_{\lambda_c}} \Delta[H_2O]\right) \quad (10)$$

which means there are three equations with three unknowns. Equations (4) through (10) assumes a homogeneous change in the absorption of the medium and a known value of photon path length (ld_p) [**47**]. In reality, there is a spatial inhomogeneity in the tissue absorption changes, and therefore the first assumption proves to be invalid. There are systematic errors of two kinds in this phenomenon: (i) the partial volume effect, in which the above formulae underestimate the concentration changes, and (ii) the cross-talk taking place between chromophores in tissues particularly due to dynamic changes in their concentrations. A survey of literature reveals combinations of optimal wavelength being reported for the dual wavelength case, where these errors are very less [**48, 49**]. However, it is difficult to directly measure the photon path-length due to reflection and refraction taking place in the various tissue layers. Unless path-length is determined, only relative change in chromophore concentration can be assessed. Computer simulation and modeling may be used to estimate optical path-length through the tissues. Using techniques such as successive approximation, an analysis algorithm can be designed and calibrated to obtain a relatively accurate measure of absolute change in chromophore concentration, as implemented in some commercial devices.

Deoxy-hemoglobin (Hb) exhibits a significant absorption in the wavelength range of 650nm to 1000nm. Oxy-hemoglobin (HbO2) shows an absorption peak, which lies in NIR band (700 to 1150nm). The NIR optodes used in commercially available devices are selected to be sensitive to the respective chromophores in blood and generally exhibit peak responses in the wavelength window of 700 nm to 850 nm. In case of oximetry analysis, the absorption spectra of Hb and HbO_2 are chosen to be widely separated and there is very minimal overlap with H_2O. Hb/HbO_2 shows an isobestic point at 810 nm. In order to measure total tissue hemoglobin concentration, the isobestic absorption spectra can be utilized.

A completely different approach based on radiative transport theory or frequency domain NIRS (fdNIRS) or time domain NIRS (tdNIRS) is used to measure absolute tissue chromophore concentrations. In theory, fdNIRS or tdNIRS approaches do not need to determine the actual photon path-length [**48,49**]. These techniques use multi-wavelength NIRS to measure the tissue absorption coefficients. The absorption coefficient μ is given by:

$$\mu = c\varepsilon \quad (11)$$

Thus the concentration of tissue chromophores concentration can be absolutely measured without determining optical path-length [**50**]. It has been found that this approach yields reasonable fidelity making use of an in vitro model of human skull and brain, but concentration of hemoglobin [**51**] yields ~15% error and on increase of skull thickness, the error reaches as high as 32% [**50**]. Accordingly, correction for extra-cerebral tissue is needed even with such "absolute" measurements.

Effects of extra-cerebral tissue on cerebral oxygenation

In case of transcutaneous NIRS, the photons have to travel through a heterogeneous tissue field comprising of arteries, veins, and capillaries as well as non-vascular tissues. For NIRS performed on cerebral tissue, photons will have to pass through several layers of tissue which includes scalp, skull, and meninges, containing various concentrations of blood and chromophores derived from tissues. Simulation and experimental tissue models of transcranial near infrared radiation transmission established an elliptical photon distribution which is centered on the transmitter and having mean depth proportional to separation of optodes by a factor of ~1/3 [**51**]. Increasing the distance between transmitter and receiver increases depth of penetration and also diminishes the effect of extra-cerebral tissue [**51**]; but the transmitter power must be very limited to prevent the damage of tissue due to direct radiant heat. Because the signal intensity varies inversely as the square of the path-length, a maximum separation of 5cm between the optodes is maintained [**52**]. This ensures that the NIR radiation has a mean penetration depth of ~1.7 cm and thereby giving increased weightage to cerebral versus extra-cerebral tissue [**52**]. Additional techniques must be utilized to deal with significant attenuation that is still there from extra-cerebral tissue [**53**].

Since the photons penetrate by an average depth approximately equal to 1/3 of the separation between the transmitter and receiver, therefore, two differentially spaced receiving optodes may be utilized—one spaced closer to the transmitter and the other spaced somewhat

farther from the transmitter. This yields a degree of spatial resolution. Accordingly, the nearer receiver (e.g. 3 cm separation) detects signals from primarily the superficial tissue, whereas the farther optodes (e.g. 4 cm separation) detects signals from deeper tissue. A subtraction algorithm enables calculating the difference between the shorter separation and longer separation NIRS signals and thus indicates a measure of oxygen saturation in the deeper, cortical tissue. Thus we can discriminate between the signals from cerebral and extra-cerebral tissue. Also, this demonstrates the penetration of transcutaneous photon to the depth of the cerebral ventricles [**52**]. Estimations reveal that ~85% of rSO_2 is obtained from deeper cortical tissue while the remaining ~15% is obtained from superficial extra-cerebral tissue.

Cerebral NIRS systems measure average tissue oxygen saturation and, therefore, reflect oxy-hemoglobin saturation in arterial, venous, and capillary blood consisting of the sampling volume. The distribution of mean tissue hemoglobin, in case of cerebral cortex, is 70% venous and 30% arterial [**54**]. The above observations are based on correlations observed between results of position emission tomography (PET) and NIRS [**52**]. The clinical studies, however, have revealed that individual cerebral arterial/venous (A/V) ratios between subjects vary considerably. This further emphasizes that the use of a fixed (A/V) ratio may produce significant deviation from actual tissue oxygen saturation obtained in vivo, thus confounding even "absolute" measures of rSO_2, like fdNIRS or tdNIRS [**55**]. Further, if there is variation in hemoglobin concentration due to hemo-dilution, which may lead to changes in rSO_2 without alterations of attendant in jugular venous oxygen saturation [**56**], another error gets introduced. However, the implications of this are not clear. It can indicate to subclinical regional ischemia, or changes in photon path-length or changes in cerebral A/V partitioning, or other factors [**56,57**]. In clinical practice, cerebral NIRS is used to monitor along with interventions specifically designed to preserve rSO_2values close to the baseline values. This has minimized the incidence of adverse clinical effects in patients undergoing coronary artery bypass (CAB) surgery [**58**]. Thus a trend monitoring approach diminishes confounds introduced due to variation in individual cerebral A/V ratios. These leads to an 'offset' in the results obtained.

Phenomological model for capturing hemodynamic response to anodal tDCS using NIRS

Anodal tDCS may be used to probe the CBF regulation. Here anodal tDCS produces a vasoactive stimulus which may be used to observe the system response. In this experiment, CVR is estimated as the variation in CBF per unit change in relation to intensity of anodal tDCS. A review of earlier work reveals a significant match between the strength of tDCS and regional CBF increase during the tDCS on-period as compared to the baseline before stimulation [**59**]. In our prior work, we attempted to estimate the regional CVR post anodal tDCS by suitably modifying an arteriolar compliance model depicting the cerebral blood flow in response to a neural stimulus [**60**]. Regional CVR has been defined as "the coupling between changes in CBF and cerebral metabolic rate of oxygen (CMRO2) during anodal tDCS-induced local brain activation" [**67**]. tDCS alters the synaptic transmembrane current *u(t)* (considering only the excitatory effects) via a complex path [**61**] leading to an alteration in the concentration of different vasoactive agents such as K^+ ions, adenosine, NO, etc. This can be represented by a single vasoactive signal, *S*, that induces a vascular flow. This has been captured by Friston in his famous first-order model [**62**].

$$\dot{s} = \varepsilon u(t) - k_s s - g_f(f - 1) \tag{12}$$

where ε refers to the neuronal efficacy, f indicates CBF normalized with respect to baseline value, k_s refers to the rate constant for the decay of signal amplitude with respect to time, and g_f indicates the gain constant meant for a feedback term which is auto-regulatory that feeds the CBF back to its baseline value (at steady state: $\dot{s} = 0$, $s = 0$ and $u(t) = g_f (f - 1) / \varepsilon$). The vasoactive signal, *s*, when released changes the arteriolar compliance, *C*, of the vasculature being approximated by the first-order kinetics, leading to alterations in its radius, *R*, that can be represented by a nonlinear compliance model [**60**]. For ease in NIRS data fitting, the nonlinear compliance model has been linearized about an equilibrium point C_M, and the radius, *R*, has been approximated as,

$$\dot{C} = s$$
$$R \approx R_{\max}(1 - a_1 \exp(-a_2 C_M)) \tag{13}$$

where $R_{\max}$ refers to the maximum radius of artery, and a_1 and a_2 are constants. The CBF can be approximated using an Ohmiclike equation,

$$CBF = K(P_a - P_v)R^{\gamma} \tag{14}$$

where P_a is the arterial blood pressure, P_v is the venous blood pressure, K is a proportionality constant, and the exponent γ is 4 for laminar flow and 2 for plug-flow. Anodal tDCS is assumed to cause change in CBF through changes in synaptic transmembrane current, *u(t)*, leading to alterations only in *R* and not in blood pressure difference ($P_a - P_v$). However, tDCS has bihemispheric effects on cerebral vasomotor reactivity [**63**] which causes an additional systemic effect which we neglected to simplify the model. Under this simplified assumption, the baseline-normalized CBF, *f*, can be approximated as

$$f = \left(\frac{R}{R_0}\right)^{\gamma} \tag{15}$$

where R_0 is the tissue vasculature radius at baseline. Since NIRS measures alterations in oxy-hemoglobin -(*HbO2*), and deoxy-hemoglobin (*Hb*) concentration in tissues, these parameters require to be approximated based on the value of *f*. So a new hemodynamic variable, *Hbt*, has been derived as the sum of the concentrations of *HbO2* and *Hb*,

which reasonably indicates variations of regional cerebral blood volume, Vol_{blood} [**64**]. It is assumed that the vasculature of tissue has a volume, Vol_{vasc}, which is proportional to R^2. The haematocrit remaining constant, the change in total (*Hbt*) hemoglobin concentration in tissues can be approximated as [**65**].

$$\frac{Vol_{vasc}}{Vol_{vasc,0}} = \frac{R^2}{R_0^{\,2}}$$
$$\Rightarrow \frac{Vol_{blood}}{Vol_{blood,0}} = \frac{R^2}{R_0^{\,2}}$$
$$\Rightarrow \frac{Hbt}{Hbt_0} = \frac{R^2}{R_0^{\,2}}, \because \text{ haematocrit constant}$$
$$\Rightarrow f = \left(\frac{Hbt}{Hbt_0}\right)^{\gamma/2} \tag{16}$$

The "cerebral metabolic rate of oxygen", *CMRO2* (i.e., oxygen consumption), is given by "the difference of oxygen flowing into and out of the tissue" [**65**]. Assuming that the oxygen concentration in arteries, C_A, is not affected by anodal tDCS [**60**], *CMRO2* may be related to CBF as,

$$CMRO2 = E \cdot C_A \cdot CBF$$
$$\Rightarrow \frac{CMRO2}{CMRO2_0} = \frac{E(f, E_0)}{E_0} f \tag{17}$$

where *E* refers to the oxygen extraction fraction (E_0 at baseline). CVR was defined as the "ratio between fractional CBF change and fractional CMRO2 change from baseline" [65],

$$CVR = \frac{CMRO2 / CMRO2_0}{f} \Rightarrow CVR = \frac{E(f, E_0)}{E_0}$$

The baseline-normalized CMRO2 (i.e. CVR·*f*) is estimated from the baseline-normalized tissue CBF *(f)*, and deoxy-hemoglobin (*Hb*) and total (H*bt*) hemoglobin concentration using the ratio method [**65**],

$$\left(1+\frac{CMRO2}{CMRO2_0}\right) = (1+f)\left(1+\gamma_R \frac{Hb}{Hb_0}\right)\left(1+\gamma_T \frac{Hbt}{Hbt_0}\right)^{-1} \text{ from [19]}$$
$$\Rightarrow (1+CVR \cdot f) = (1+f)\left(1+\gamma_R \frac{Hb}{Hb_0}\right)\left(1+\gamma_T \frac{Hbt}{Hbt_0}\right)^{-1}$$
$$\Rightarrow \left(1+CVR \cdot \left(\frac{Hbt}{Hbt_0}\right)^{\gamma/2}\right) = \left(1+\left(\frac{Hbt}{Hbt_0}\right)^{\gamma/2}\right)\left(1+\gamma_R \frac{Hb}{Hb_0}\right)\left(1+\gamma_T \frac{Hbt}{Hbt_0}\right)^{-1} \tag{18}$$

Here, the factors $\gamma_R \in [0.5, 1.5]$; $\gamma_T \in [0.5, 1.5]$ establishes a relationship between fractional hemoglobin changes in the venous compartment and those across all vascular components. $SO2_0$ relates saturation of oxygen at baseline of the venous compartment to Hbt_0 [**66**]),

$$SO2_0 = \frac{HbO2_0}{Hb_0 + HbO2_0} \Rightarrow SO2_0 = \frac{Hbt_0 - Hb_0}{Hbt_0} \tag{19}$$

If there is a diffusion-limited oxygen delivery [**66**], the consumption of oxygen is limited by diffusion of oxygen from the vasculature. Hence, consumption of oxygen is tightly coupled to induced flow of blood [**65**] and the surface area of the vasculature which is proportional to *R*. A neural mass model [**68**] relating intensity of anodal tDCS (current density), $\sigma(t)$, to tDCS-induced changes in synaptic transmembrane current, $u(t)$ [**61**] can be incorporated with the neurovascular model (i.e., equations 1-4) representing the total hemodynamic (*Hbt*) response to anodal tDCS, $\sigma(t)$, where deoxy-hemoglobin (*Hb*) is a by-product of the consumption of oxygen delivered by oxy-hemoglobin (*HbO*2) that can be estimated using *CMRO*2 [**68**].

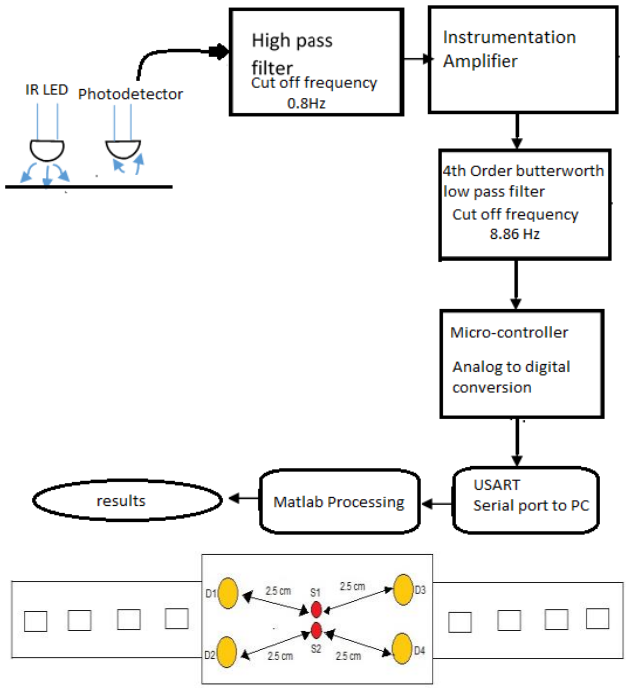

Fig. 3. Top Panel: Block diagram of the NIRS system. Bottom Panel: Design of NIRS probe.

Design of the NIRS device

A NIRS device has been developed in our lab, the design of which is shown in **Fig. 3**. The NIRS device comprises of four sources (having a range of 770 nm and 850 nm) and three photo-detectors. Since, NIRS is an optical measurement technique, therefore, the changes in the optical properties of the volume of tissue induces signal changes during neural activation. This entails for a spectro-photometric modeling component to capture the dynamics of the signal. The signal being received at the detector can be reasonably estimated as a linear mixing of a large number of signal components. In order to obtain relative values of changes in the concentrations of the two oxygenation related chromophores, namely oxy-hemoglobin and deoxy-hemoglobin, differential spectroscopy has been used, which makes it possible to determine whether changes in oxygen saturation happen due to alterations in blood volume or variations in the consumption of oxygen. A change in blood volume causes a proportional change in total hemoglobin concentration which again leads to a change in oxygen saturation.

Changes in the consumption of oxygen are specified by changes in chromophores concentrations in mutually opposite directions resulting in the total hemoglobin concentration remaining the same. Two wavelengths of 770nm and 850 nm were used in the experiment. The sources and photo-detectors were aligned as presented in **Fig. 3**. S1 and S2 indicate the position of sources and D1, D2, D3 and D4 indicate the position of photo-detectors.

In anodal tDCS a constant weak direct current is delivered transcranially through spongy conductive rubber-core electrode, where the spongy electrode is soaked in normal (0.9%) saline solution. 0.526A/m^2 of current density has been delivered due to anodal tDCS for the duration of 3 minutes. The anode has been placed at Cz site of scalp ("International 10-20 system of scalp sites") and the cathode has been placed at either F3 or F4 site for left and right hemispheric stimulations respectively. The developed NIRS device is used to extract the signal from both sides of the cerebral frontal cortex both before and after anodal tDCS. 15 subjects in the age group of 20-30 years were tested to determine the feasibility of hemodynamic response to anodal tDCS at the International Institute of Information Technology - Hyderabad, India [**69**]. Our hypothesis that reduced tDCS-evoked hemodynamic response would be generated by the lesioned hemisphere was evaluated in 14 stroke survivors of the age group of 42-73 years, at the Institute of Neurosciences, Kolkata [**69**].

Following a formal Ethics Committee approval, stroke patients were recruited after taking informed consent, conforming to the *Declaration of Helsinki*. During the trials, the subjects were seated in a silent room with their eyes focused on a dot mark on the wall in front of them. The time needed for testing was around 14 minutes. Here, NIRS was initially performed on the F3 site of the recruits for two minutes. This was followed by application of anodal tDCS for three minutes. Post anodal tDCS, again NIRS was applied to measure the variations in hemodynamics changes as a consequence of anodal tDCS. Hence, the NIRS data was recorded for 2 minutes before and after tDCS. The whole process was then repeated with F4 site of scalp. Both the NIRS signals and the analog arterial pressure data from the hemodynamic monitor of operating room were sampled at 60 Hz. Integration has been performed with these signals as non-overlapping 10 sec mean values. This is similar to a non-overlapping type moving average filter with a time window of 10 sec re-sampled at 0.1 Hz. The basic objective behind such a kind of signal processing was to remove high frequency noise from respiratory and pulse frequencies so that detection of transients and oscillations below 0.05 Hz can be allowed. Further, the resulting signals were filtered with a high pass filter having a cut off frequency of 0.003Hz. This is done to remove very slow drifts. The variation in the signal to noise ratio (SNR), in the overall NIRS signal, between the on phase and off phase of the anodal tDCS was examined. The background noise was recorded when the device was not brought in contact with the skin. A paired t-test (MATLAB function "t-test") has been performed to find any significant variation in the SNR values between the on state and off state of the anodal tDCS. The paired t-test was done to confirm hemodynamic response to tDCS in 15 healthy subjects in the age group in between 20 and 30 years. Then, 14 patients (10 male and 4 females from age 42 to 73) with established and acute ischemic stroke (less than a month) with the ischemic site localized to a single cerebral hemisphere were selected to study the effect of anodal tDCS on the hemodynamic response of the lesioned and non-lesioned hemisphere during perturbation with anodal tDCS [**69**]. A paired t-test (MATLAB function "t-test") was performed to find any significant difference. In the 14 acute ischemic stroke (less than 1 month) survivors (the lesioned hemisphere with impaired circulation displayed significantly less increase in cerebral oxygen saturation than the non-lesioned side post anodal tDCS. The non-lesioned side showed the following HbO2 concentration [male: (3.43±0.86) and female: (3.32±0.74)]. However, it was not in the side with stroke lesion [male: (0.26 ± 0.28) and female: (0.24±0.26)], $p<0.01$.

Fig. 4 shows the regional change in *HbO*2, *Hb*, and total *Hbt* concentration from 0 to 60 sec due to the application of 0.526A/m^2 ($\sigma_{norm}(t)=1$) anodal tDCS from 0-30 sec.

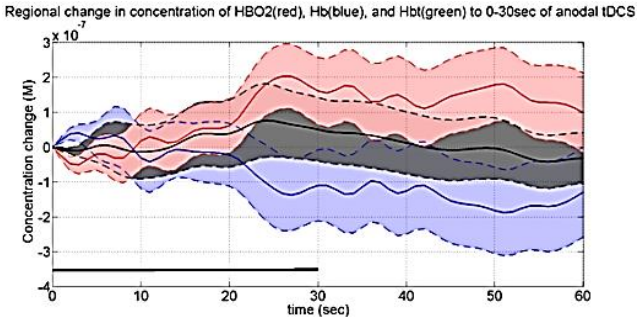

Fig. 4. Regional change in cerebral oxy-hemoglobin and deoxy-hemoglobin concentration.

Table 1. Summary of the case series (M: male, F: female, MCA: middle cerebral artery, CABG: coronary artery bypass graft).

Case	Age/ Gender	MRI diagnosis	Comorbidities	Year of stroke
1	31/M	Right MCA	White matter hyperintensities	2008
2	63/M	Left MCA	Diabetes mellitus, hypertension	2009
3	73/M	Left MCA	Post CABG	2010
4	76/F	Right MCA	Post CABG	2009

The Ischemic stroke studies were conducted on four chronic (more than 6 months) ischemic stroke survivors (3 males, 1 female from age 31 to 76 (see **Table 1**). The subjects were studied for oxy- and deoxy-hemoglobin

concentration at the University of Medicine Goettingen, Germany and the Institut national de recherche en informatique *et en.*, automatique, France [**69**]. For the four stroke cases (NIRS/EEG-tDCS stroke study), the **Fig. 5** displays the variation in *HbO*2 concentration at the lesioned and non-lesioned hemispheres of the subject from 0-60 sec during the application of anodal tDCS of current density 0.526 A/m^2 from 0-30 sec.

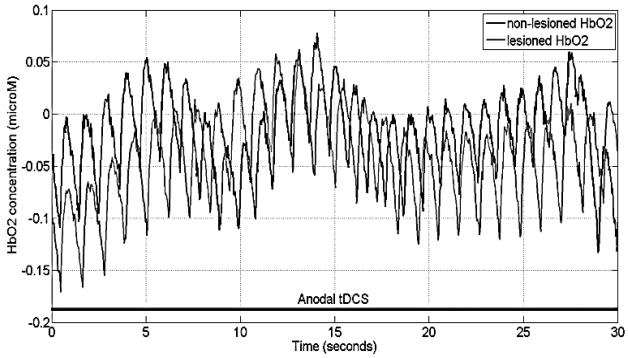

Fig. 5. Change in tissue Hb and HbO2 concentration at the lesioned and non-lesioned cerebral hemispheres.

Discussions

Alterations in oxy- and deoxy-hemoglobin concentrations at the time of anodal tDCS-induced stimulation of cerebral cortex region have been recorded with NIRS. Specifically, the signals were captured from the cortical region located beneath the stimulation electrode and in-between the light sources and detector [**70**]. The feasibility of performing anodal tDCS induced NIRS recording was confirmed by NIRS-tDCS healthy study. CVR has been captured with NIRS device [**71**]. It was further postulated that alterations in cerebral hemodynamics are causally related to neural alterations induced by anodal tDCS in cortical excitability through neuro-vascular coupling (NVC). In fact, a phenomological model was developed to estimate the regional CVR during anodal tDCS [**71**]. In [**60**] the phenomological model was developed adapting an arteriolar compliance model. This model is based on cerebral blood flow response to the applied neural stimulus [**60**]. The regional CVR has been defined as "the coupling between changes in cerebral blood flow (CBF) and cerebral metabolic rate of oxygen (CMRO2) during anodal tDCS-induced local brain activation" [**67**]. The current NIRS study estimates the average SNR of the NIRS device to be 42.33 ± 1.33dB during the on state of tDCS and 40.67 ± 1.23dB during the off state of tDCS (see **Table 2**). In the study the difference between on state and off state of tDCS was found to be statistically significant ($p<0.01$). Also, one of the 15 healthy subjects was found to have the cerebral oxygenation level in the range of 60-69%. A clinical study conducted on 14 stroke patients has revealed that the response to anodal tDCS in lesioned hemisphere with impaired circulation shows significantly less change in cerebral oxygenation ($p<0.01$) than the non-lesioned hemisphere.

Table 2. SNR of 15 healthy subjects during on and off tDCS phases.

Subject Id	Off-tDCS SNR (dB)	On-tDCS SNR (dB)
1	38.0721	39.9504
2	39.4715	41.5991
3	39.8311	41.3332
4	42.384	43.2835
5	41.2198	42.3838
6	39.5062	40.6702
7	40.819	42.5564
8	42.2779	45.4101
9	41.1092	42.3265
10	42.1952	44.1645
11	40.2977	42.4342
12	42.0211	42.963
13	40.1072	42.1107
14	40.1425	41.5978
15	40.5357	42.1622

However, it is not clear as to how tDCS acts on NIRS because a recent study using unilateral anodal tDCS revealed consensual changes in heart rate variability [**72**]. In [**73**], the correlation of arterial blood pressure and *Hbt* has been measured at low frequencies with the help of NIRS. This correlation is an index of CVR [**73**]. NIRS has been used to obtain analogy arterial pressure data from operating room hemodynamic monitor. This data is currently under study to understand the mechanisms. Moreover, an initial dip in *HbO*2 has been observed at the initial phase of of anodal tDCS [**74**]. The initial dip in *HbO*2 is hypothesized to be due to a fast increase in *Hbt* due to vasodilation. Here the value of the initial dip may indicate the temporal interplay of monophasic *Hb*, *HbO*2 and *Hbt* signals, as elucidated by Sirotin *et al.*, [**75**]. This initial dip is found to be temporally and spatially correlated with an increase in the log-transformed mean-power of EEG within frequency band of 0.5Hz-11.25Hz and may serve as a biomarker of cerebral micro vessel functionality (and NVC) [**70,74**]. A phenomological model [**71**] has been proposed based on the Friston's first order model [**62**] where it has been shown that anodal tDCS effected changes in synaptic transmembrane current leading to a change in CBF via a simultaneous change in the representative radius of arterial vasculature, and not in arterial and venous blood pressure difference. The proposed phenomological model assumed that the variations in baseline *HbO*2 at the time of anodal tDCS were only due to local hemodynamic effect. Also, the local hemodynamic effect was induced by anodal tDCS and was not due to variations in arterial oxygen concentration. However, to comprehend the underlying mechanisms in details, the NIRS-EEG joint imaging technique is presented in [**74**]. This technique may help in developing a simplified model which depicts the complex pathway of NVC from a variation in synaptic transmembrane current. This change occurs due to a change in the concentration of multiple vasoactive agents (such as K^+ ions, NO, adenosine). This variation is

represented by a single vascular flow-inducing vasoactive signal, which is based on the first-order Friston's model [**62**].

In this study, however, it has been assumed that the spatially resolved spectroscopy technique removes skin blood flow artifacts from the NIRS signal. But this assumption has to be validated appropriately with the time-gated optical system for depth-resolved NIRS [**76**]. To remove superficial extra-cortical contributions in the NIRS signal, short separation NIRS channels can be added [**77**]. However, NVC estimation based on joint NIRS-EEG analysis revealed interplay between impaired cerebro-vascular circulation and impaired neuronal response to applied anodal tDCS in the study which is hypothesized to be robust to superficial extra-cortical contributions (e.g. CCF analysis may filter out electromyogram and skin blood flow artifacts). This needs to be investigated further for the development of a robust biomarker for impaired cerebral microvessels and impaired neuronal functionality prior to stroke or cerebro-vascular accident. Such impairments have been found to be strongly correlated with elevated risk of ischemic stroke. These may help in identifying risk of stroke in patients with high-grade stenosis or occlusion in internal carotid artery. Moreover, it is hypothesized that the level of NVC, approximated using simultaneous NIRS-EEG recordings, may be used for titrating anodal tDCS as an adjuvant treatment to increase blood perfusion in the lesioned region and surrounding ischemic penumbra by increasing regional CBF [**71**]. This results in a non-invasive bedside intervention device which can localize the impaired cerebro-vascular circulation and impaired neuronal response in ischemic patients suffering from stroke and then target the same with anodal tDCS. Here, the frequency, symmetry and reactivity of hemodynamic and neuronal responses evoked with tDCS may be the used as a biological marker for the respective field studies in future. Currently robust fault tolerant algorithms for sensors are being developed for EEG-NIRS sensor data fusion based on Kalman filters [**59**].

Conclusion

This review elucidates the "versatility" of NIRS in cerebral oxygenation studies with emphasis on recent works. A survey of literature reveals a plethora of research activities being carried out in the field of near infrared spectroscopy as applied to cerebral oxygenation studies. The study on healthy and stroke patients revealed detectable hemodynamic and neuronal changes to anodal tDCS of current density 0.526 A/m^2 which demonstrated the feasibility of this approach. Moreover, it was verified in stroke survivors that the lesioned hemisphere with impaired cerebro-vascular circulation responded with significantly less variation in cerebral oxygenation ($p < 0.01$) than the non-lesioned side to anodal tDCS. Therefore, it can be concluded that anodal tDCS can perturb local neuronal and cerebro-vascular activity (via NVC) which can be used for gauging regional cerebral microvessels functionality in which clinical studies are compulsory in small vessel diseases for validation.

Ethical declaration statement

Ethical standards

The patient data and analysis of the same have been carried out with approval of Ethics Committee of IIT Mandi and the Institute Review Board (IRB) of Institute of Neurosciences, Kolkata.

Acknowledgment

The authors would like to acknowledge the support lent by Institute of Neurosciences Kolkata, Embedded Systems Lab at IIIT Hyderabad and Biomedical Systems Lab at IIT Mandi for enabling to carry out the necessary experiments for this project.

Keywords

Near infrared spectroscopy, cerebral hemodynamics, cerebral oxygenation, cerebrovascular reactivity, transcranial direct current stimulation.

Received: 24 July 2019
Revised: 19 February 2020
Accepted: 19 February 2020

References

1. Siesler, H. W.; Y. Ozaki, S. Kawata, H. M. Heise (Ed.), "Near-Infrared Spectroscopy", **2002**, Wiley-VCH, Weinheim.
2. Y. Ozaki, W. F. McClure, and A. A. Christy (Ed.), "Near Infrared Spectroscopy in Food Science and Technology", **2006**, Wiley Interscience, New York.
3. Workman, J.; Weyer, L.; "Practical Guide to Interpretive Near Infrared Spectroscopy", **2007**, CRC Press, Boca Raton.
4. Workman J.; Weyer, L.; "Practical Guide and Spectral Atlas for Interpretive Near-Infrared Spectroscopy, Second Edition", **2012**, CRC Press, Boca Raton.
5. Ciurczak, E. W.; Drennen, J. K.; III, "Pharmaceutical and Medical Applications of Near-Infrared Spectroscopy", **2002**, CRC Press, Boca Raton.
6. Roberts, C. A.; "Near-infrared Spectroscopy in Agriculture", **2004**, American Society of Agronomy.
7. Williams, P. C.; "Near-infrared Spectroscopy", **1996**, NIR Publications, Chichester, UK.
8. Tichauer, K.; "Near-Infrared Spectroscopy: Diagnosis of Neonatal Hypoxia-Ischemia", **2010**, VDM Verlag.
9. Burns, D. A.; Ciurczak, E. W.; (Ed.), "Handbook of Near-Infrared Spectroscopy", 3rd Ed., **2008**, CRC Press, Boca Raton.
10. Osborne, B. G.; Fearn, T.; "Near Infrared Spectroscopy in Food Analysis", **1986**, Longman Higher Education.
11. Figgis, B. N.; "Introdution to Lifand Fields", **1966**, Krieger Pub. Co.
12. Villringer, A.; Dirangl, U.; (Ed.), "Optical Imaging of Brain Function and Metabolism 2", **1997**, Springer, Berlin.
13. Ciurczak, E. W.; in "Handbook of Near-Infrared Analysis", Ed. D. Burns, A.; Ciurczak, E. W.; 3rd Ed., **2008**, CRC Press, Boca Raton, 647.
14. Llusar, M.; Badeness, A.; Calbo, J.; Tena, M. A.; Monros, G.; *J. Eur. Ceram. Soc*., **2001**, *21*, 1121.
15. Candeia, R. A.; Souza, M. A. F.; Bernardi, M. I. B.; Maestelli, S. C.; Santos, I. M. G.; Souza, A. G.; Longo, E.; *Mater. Res. Bull*., **2006**, *41*, 183.
16. Jobsis, F.F.; Noninvasive, infrared monitoring of cerebral and myocardial oxygen sufficiency and circulatory parameters. Science **1977**, *198*, 1264–7.
17. Chance, B.; Zhuang, Z.; UnAh, C.; Alter C.; Lipton, L.; *Proc. Natl. Acad. Sci. U. S. A.*, **1993**, *90*, 3770.
18. Arenth, P. M.; Ricker J. H.; Schultheis, M. T.; *Clin. Neuropsychol.*, **2007**, *21*, 38.

19. Strangman, G.; Goldstein, R.; Rauch, S. L.; Stein, J.; *Arch. Phys. Med. Rehabil.*, **2006**, *87*, S12-9.
20. Hamaoka, T.; McCully, K. K.; Quaresima, V.; Yamamoto, K.; Chance, B.; *J. Biomed. Opt.*, **2007**, *12*, 062105.
21. Carpenter, C. M.; Srinivasan, S.; Pogue, B. W.; Paulsen, K. D.; *Opt. Express*, **2008**, *16*, 17903.
22. Liu, H.; Song, Y.; Worden, K. L.; Jiang, X.; Constantinescu, A.; Mason, R. P.; *Appl. Opt.*, **2000**, *39*, 5231.
23. Franceschini, M. A.; Nissila, I.; Wu, W.; Diamond, S. G.; Bonmassar G.; Boas, D. A.; *NeuroImage*, **2008**, *41*, 189.
24. Ou, W.; Nissila, I.; Radhakrishnan, H.; Boas, D. A.; Hamalainen, M. S.; Franceschini, M. A.; *NeuroImage*, **2009**, *46*, 624.
25. Franceschini, M. A.; Thaker, S.; Themelis, G.; Krishnamoorthy, K. K.; Bortfeld, H.; Diamond, S. G.; Boas, D. A.; Arvin, K.; Grant, P. E.; *Pediatr. Res.*, **2007**, *61*, 546.
26. Coyle, S. M.; Ward, T. E.; Markham, C. M.; *J. Neural Eng.*, **2007**, *4*, 219.
27. Dalal, P. M.; *et al.*, *Neuroepidemiology*, **2008**, *31*, 254.
28. Das, S. K.; *et al.*, *Stroke*, **2007**, *38*, 906.
29. Sridharan, S. E.; *et al.*, *Stroke*, **2009**, *40*, 1212.
30. Lopez, A. D.; Mathers, C. D.; Ezzati, M.; Jamison, D. T.; Murray, C. J.; *Lancet*, **2006**, *367*, 1747.
31. Benesch, C.; Holloway, R. G.; *CNS Drugs*, **1998**, *9*, 29.
32. Go, A. S.; *et al.*, *Circulation*, **2014**, *129*, e28.
33. Tripathi, M.; Vibha, D.; *Stroke Res. Treat.*, **2010**, 2011.
34. Das, A.; Botticello, A. L.; Wylie, G. R.; Radhakrishnan, K.; *Neurology*, **2012**, *79*, 2146.
35. *WG-3.2 Non-Communicable Diseases Report*. [Online]. Available: http://planningcommission.nic.in/aboutus/committee/wrkgrp12/health/WG_3_2non_communicable.pdf, accessed Aug. 23, **2014**.
36. Markus. H.; Cullinane, M.; *Brain*, **2001**, *124*, 457.
37. Hossmann, K. A.; *Ann. Neurol.*, **1994**, *36*, 557.
38. Astrup, J.; Siesjö, B. K.; Symon, L.; *Stroke*, **1981**, *12*, 723.
39. Goldstein, L. B.; *Drug Safety*, **2000**, *22*, 13.
40. Dawson, S. L.; Panerai, R. B.; Potter, J. F.; *Cerebrovascular Diseases*, **2003**, *16*, 69.
41. Girouard, H.; Iadecola, C.; *J. Appl. Physiol.*, **2006**, *100*, 328.
42. Silvestrini, M.; *et al.*, *Stroke*, **2006**, *37*, 1010.
43. Lloyd-Fox, S.; Blasi, A.; Elwell, C. E.; *Neurosci. Biobehavioral Rev.*, **2010**, *34*, 269.
44. Douds, M. T.; Straub, E. J.; Kent, A. C.; Bistrick, C. H.; Sistino, J. J.; *Perfusion*, **2014**, *29*, 545.
45. Villringer, A.; Chance, B.; *Trends Neurosci.*, **1997**, *20*, 435.
46. Beer, A.; *Annalen der Physik und Chemie*, **1852**, *86*, 78.
47. Obrig, H.; Villringer, A.; *J. Cereb. Blood Flow Metab.*, **2003**, *23*, 1.
48. Strangman, G.; Franceschini M.A.; Boas, D.A.; *Neuroimage*, **2003**, *18*, 865.
49. Uludag, K.; Steinbrink, J.; Villringer, A.; Obrig, H.; *Neuroimage*, **2004**, *22*, 583.
50. Kurth, C.D.; Thayer, W.S.; *Phys. Med. Biol.*, **1999**, *44*, 727.
51. Germon, T.J.; Evans, P.D.; Barnett, N.J.; Wall, P.; Manara, A.R.; Nelson, R.J.; *Br J Anaesth*, **1999**, *82*, 831.
52. Ohmae, E.; Ouchi, Y.; Oda, M.; et al., *Neuroimage*, **2006**, 29, 697.
53. Murkin, J.M.; Arango, M.; *Br J Anaesth*, **2009**, *103*, i3.
54. McCormick, P.W.; Stewart, M.; Goetting, M.G.; Balakrishnan, G.; *Stroke*, **1991**, *22*, 596.
55. Watzman, H.M.; Kurth, C.D.; Montenegro, L.M.; Rome, J.; Steven, J.M.; Nicolson, S.C.; *Anesthesiology*, **2000**, *93*, 947.
56. Yoshitani, K.; Kawaguchi, M.; Iwata, M.; et al., *Br. J. Anaesth*, **2005**, *94*, 341.
57. Pattinson, K.T.; Imray, C.H.; Wright, A.D.; *Br. J. Anaesth*, **2005**, *94*, 863.
58. Murkin, J.M.; Adams, S.J.; Novick, R.J.; et al., *Anesth Analg*, **2007**, *104*, 51.
59. Zheng, X.; Alsop, D.C.; Schlaug, G.; *Neuroimage*, **2011**, 58, 26.
60. Behzadi, Y.; Liu, T.T.; *Neuroimage*, **2005**, *25*, 1100.
61. Molaee-Ardekani, B.; et al., *Brain Stimul.*, **2013**, *6*, 25.
62. Friston, K.J.; et al., *Neuroimage*, **2000**, *12*, 466.
63. Vernieri, F.; Assenza, G.; Maggio, P.; Tibuzzi, F.; Zappasodi, F.; Altamura, C.; et al., *Stroke J. Cereb Circ.*, **2010**, 41, 2087.
64. Villringer, A.; Chance, B.; *Trends Neurosci.*, **1997**, *20*, 435.
65. Boas, D.A.; Strangman, G.; Culver, J.P.; Hoge, R.D.; Jasdzewski, G.; Poldrack, R.A.; et al. *Phys. Med. Biol.*, **2003**, *48*, 2405.
66. Buxton, R.B.; Frank, L.R.; *J. Cereb. Blood Flow Metab.*, **1997**, *17*, 64.
67. Leontieva, O.; Buxton, R.B.; *Neuroimage*, **2007**, *35*, 175.
68. Dutta, A.; Nitsche, M.A.; "Neural mass model analysis of online modulation of synaptic mechanisms with transcranial direct current stimulation," IEEE NER, ***2013***.
69. Jindal, U.; Sood, M.; Dutta, A.; Chowdhury, S. Roy; *IEEE Journal of Translational Engineering in Health and Medicine*, **2015**, *3*, 1.
70. Dutta, A.; "EEG-NIRS based low-cost screening and monitoring of cerebral microvessels functionality", in Proc. Int. Stroke Conf., **2014**.
71. Dutta, A.; Chowdhury, S. R.; Dutta, A.; Sylaja, P. N.; Guiraud, D.; Nitsche, M. A.; "A phenomological model for capturing cerebrovascular reactivity to anodal transcranial direct current stimulation," in Proc. 6th Int. IEEE/EMBS Conf. Neural Eng. (NER), Nov. **2013**, pp. 827-830.
72. Montenegro, R. A.; *et al.*, *Neurosci. Lett.*, **2011**, *497*, 32.
73. Lee J. K.; *et al.*, *Stroke*, **2009**, *40*, 1820.
74. Dutta, A.; Jacob, A.; Chowdhury, S. R.; Das, A.; Nitsche, M. A.; *J. Med. Syst.*, **2015**, *39*, 36.
75. Sirotin, Y. B.; Hillman, E. M. C.; Bordier, C.; Das, A.; *Proc. Nat. Acad. Sci. United States Amer.*, **2009**, *106*, 18390.
76. Barbour, R. L.; *et al.*, *Proc. SPIE*, **2008**, *6870*, 687002.
77. Koh, P. H.; Elwell, C. E.; Delpy, D. T.; "Development of a dynamic test phantom for optical topography", in Oxygen Transport to Tissue 30, Liss, P.; Hansell, P.; Bruley, D. F.; Harrison, D. K.; Eds. New York, NY, USA: Springer-Verlag, **2009**, pp. 141-146.
78. Dutta, A.; Koerding, K.; Perreault, E.; Hargrove, L.; "Sensor-fault tolerant control of a powered lower limb prosthesis by mixing mode-specific adaptive Kalman filters," in Proc. Annu. Int. Conf. IEEE Eng. Med. Biol. Soc., **2011**, Vol. 2011, pp. 3696-3699.